Mapping evapotranspiration based on remote sensing: An application to Canada's landmass

J. Liu

Canada Centre for Remote Sensing, Ottawa, Ontario, Canada
Atmospheric Science, Department of Physics, University of Toronto, Toronto, Ontario, Canada

J. M. Chen

Department of Geography, University of Toronto, Toronto, Ontario, Canada
Canada Centre for Remote Sensing, Ottawa, Ontario, Canada

J. Cihlar

Canada Centre for Remote Sensing, Ottawa, Ontario, Canada

Received 21 August 2002; revised 31 January 2003; accepted 9 April 2003; published 29 July 2003.

[1] The evapotranspiration (ET) from all Canadian landmass in 1996 is estimated at daily steps and 1 km resolution using a process model named boreal ecosystem productivity simulator (BEPS). The model is driven by remotely sensed leaf area index and land cover maps as well as soil water holding capacity and daily meteorological data. All the major ET components are considered: transpiration from vegetation, evaporation of canopy-intercepted rainfall, evaporation from soil, sublimation of snow in winter and in permafrost and glacier areas, and sublimation of canopy-intercepted snow. In forested areas the transpiration from both the overstory and understory vegetation is modeled separately. The Penman-Monteith method was applied to sunlit and shaded leaf groups individually in modeling the canopy-level transpiration, a methodological improvement necessary for forest canopies with considerable foliage clumping. The modeled ET map displays pronounced east-west and north-south gradients as well as detailed variations with cover types and vegetation density. It is estimated that for a relative wet year of 1996, the total ET from all Canada's landmass (excluding inland waters) was 2037 km^3. If compared with the total precipitation of 5351 km^3 based on the data from a medium range meteorological forecast model, the ratio of ET to precipitation was 38%. The ET averaged over Canadian land surface was 228 mm/yr in 1996, partitioned into transpiration of 102 mm yr^{-1} and evaporation and sublimation of 126 mm yr^{-1}. Forested areas contributed the largest fraction of the total national ET at 59%. Averaged for all cover types, transpiration accounted for 45% of the total ET, while in forested areas, transpiration contributed 51% of ET. Modeled results of daily ET are compared with eddy covariance measurements at three forested sites with a r^2 value of 0.61 and a root mean square error of 0.7 mm/day. *INDEX TERMS:* 0315 Atmospheric Composition and Structure: Biosphere/atmosphere interactions; 1640 Global Change: Remote sensing; 1818 Hydrology: Evapotranspiration; 1833 Hydrology: Hydroclimatology; 9350 Information Related to Geographic Region: North America; *KEYWORDS:* transpiration, evaporation, remote sensing, hydroecological modelling, hydrological process, Canada

Citation: Liu, J., J. M. Chen, and J. Cihlar, Mapping evapotranspiration based on remote sensing: An application to Canada's landmass, *Water Resour. Res.*, *39*(7), 1189, doi:10.1029/2002WR001680, 2003.

1. Introduction

[2] Quantitative information on evapotranspiration (ET) over large areas from a subcontinental to the global scale is useful for water resource management and climate studies. Spatial distributions of ET at these scales are traditionally estimated with long-term meteorological or runoff data because the available input data were often limited [*Hare*, 1980; *Willmott et al.*, 1985; *Henning*, 1989; *Mintz and Walker*, 1993; *Potter et al.*, 1993]. Because remotely sensed data have the advantage of large area coverage, frequent update and consistent quality, remote sensing based ET estimation has been a subject of many studies [*Rango*, 1989; *Kuittinen*, 1992; *Kite and Pietroniro*, 1996; *Stewart et al.*, 1996; *Sorooshian et al.*, 1997; *Rango and Shalaby*, 1999]. As ET cannot be directly measured by remote sensing technique, indirect estimation of ET using remotely sensed data has been explored with several approaches, such as the energy balance approach (or so-called the residual approach) [*Choudhury*, 1997; *Seguin*, 1997] and the Priestley-Talor or modified Priestley-Talor approach [*Jiang and Islam*, 2001]. Coupling process-based ET models with remote sensing data has emerged in the last two decades.

0043-1397/03/2002WR001680$09.00

Process-based models simulate a series of physical and plant physiological processes controlling ET, such as radiation absorption, precipitation interception, and stomatal movement. Applications of process models have been reported at scales from watersheds to the globe [*Sellers et al.*, 1986; *Running et al.*, 1989; *Band et al.*, 1991; *Wood and Lakshmi*, 1993; *Liu et al.*, 1997; *Choudhury et al.*, 1998; *Strasser and Mauser*, 2001].

[3] Process models, when used for ET mapping, have several advantages: (1) the contribution of each process to the total ET is explicitly quantified; (2) the effects of vegetation on ET are considered through the use of spatial vegetation structural data such as leaf area index, and vegetation functional parameters such as stomatal conductance; (3) the interaction between soil moisture and ET can be explicitly described; and (4) ET can be calculated for a defined period rather than as long-term averages so that its temporal variations can be studied. Process models are usually originated at a stand/plot level in various details [*Norman*, 1979; *Braud et al.*, 1995; *Pauwels and Wood*, 1999]. These models often have to be simplified when implemented over a large area because of the constraints caused by the availability of spatial data and computing resources.

[4] Depending on individual situation, process models are built with different emphasis, complexity, input requirement, and temporal and spatial resolutions. In this study, a simplified process model, namely, the boreal ecosystem productivity simulator (BEPS) [*Liu et al.*, 1997], is developed for regional ET estimation ($\sim 10^7$ km^2). BEPS underscores the importance of vegetation data, including leaf area index and vegetation type, on qualifying ET distribution. These spatially explicit vegetation data are derived from satellite data. BEPS is specifically designed for use of these remotely sensed data. Second, BEPS utilizes an approach that emphasizes more on spatial resolution while keeping the temporal resolution to its maximum with the available computing resources and input data. Finally, BEPS is focused on the vegetation, meteorology, and soil conditions in Canada. The main purpose of this paper is to show the detailed spatial distribution patterns of ET over Canada's landmass through process modeling and to quantify ET statistics in Canada for a year.

2. Model and Data

2.1. Description of the Model

[5] BEPS was originally developed for assessing carbon uptake by vegetation over Canadian landmass [*Liu et al.*, 1997, 1999, 2002]. ET simulation is evidently an important part of the model because of the close relationship between carbon uptake and water regime [*Liu et al.*, 1997, 2001]. BEPS follows and further develops the algorithms embedded in FOREST-BGC [*Running and Coughlan*, 1988] to describe the physical and biological processes in vegetation. With spatially explicit input data on vegetation, meteorology and soil, BEPS can be run pixel by pixel over a defined domain, such as Canada, or any of its parts. It has flexible spatial and temporal resolutions, as long as the input data of each pixel are defined. In this study, BEPS was run at a daily time step and 1 km resolution, while the application of daily BEPS at a 30 m resolution is reported [*Zelic et al.*, 2002] and a version of hourly BEPS at 20 km is being developed [*Chan et al.*, 2000, 2001]. The sensitivities of ET simulated by BEPS to environmental conditions and plant characteristics are demonstrated by *Potter et al.* [2001] in a comparison among nine models for a boreal forest site. Similar to most models compared, BEPS is sensitive to changes in leaf area index, stomatal conductance, air temperature and humidity at the site. In terms of the root mean square errors in comparison with measured ET data at the site, BEPS ranked the second lowest [*Amthor et al.*, 2001].

[6] In this study, BEPS calculates each ET component daily and sums the daily values to yearly ET for every pixel in a map. Given Canada's large forested and permafrost areas and long winter season, transpiration from understory vegetation in forests and sublimation of snow and ice are taken into account, in addition to other common ET components. Figure 1 shows the components considered in BEPS. The complete ET model is:

$$\mathrm{ET} = T_{plant} + T_{under} + E_{plant} + S_{plant} + E_{soil} + S_{ground} \quad (1)$$

where T_{plant} is transpiration from plants, or overstory plants (trees) for forested areas; T_{under} is transpiration of the understory in forests, equal to zero for nonforest cover types; E_{plant} and S_{plant} are evaporation and sublimation from plants, respectively; E_{soil} is evaporation from soil; and S_{ground} is sublimation from the snow on the ground. The time dependent input variables to the model are leaf area index in 10/11-day interval during the growing season and meteorological data on daily basis, including total incoming radiation, maximum and minimum temperature, mean humidity and total precipitation. Other input variables contain land cover type and available soil water holding capacity, both variant spatially but invariant temporally in one year.

[7] In compromise with limitations of available spatial data and computing resources, the following treatments were adopted: (1) environmental and plant conditions are considered as homogeneous within a pixel; (2) lateral interactions among pixels are neglected; (3) soil is treated as one layer and the moisture is calculated with the "bucket model"; (4) the remaining portion of the intercepted precipitation after evaporation or sublimation goes to soil as secondary throughfall at the end of the day; and (5) the aerodynamic resistance to water vapor is described with various representative values for different land cover types.

[8] T_{plant} is one of the major components in vegetated areas. The Penman-Monteith equation [*Monteith*, 1965] has been widely used to describe this process at an instant of time per unit leaf surface area:

$$T_{plant} = \left[\frac{\Delta R_n + \rho c_p VPD/r_a}{\Delta + \gamma(1 + r_s/r_a)}\right]/\lambda_v \quad (2)$$

where R_n is the net absorbed radiation in W m^{-2} (see Appendix for the approach to calculate R_n for overstory, understory and soil surface in estimating T_{plant}, T_{under}, and E_{soil}), Δ is the rate of change of the saturated water vapor pressure with temperature in mbar °C^{-1}; ρ is the density of air (=1.225 kg m^{-3} at 15°C); c_p is the specific heat of air at constant temperature (=1010 J kg^{-1} °C^{-1}); *VPD* is the vapor pressure deficit in mbar; r_a is the aerodynamic resistance, taken to be 30 s m^{-1} for crop and grass land and 5.0 s m^{-1} for forest and other land cover types [*Grace*, 1983; *Running and Coughlan*, 1988] (the error analysis for taking r_a as vegetation-type dependent constants is provided later in

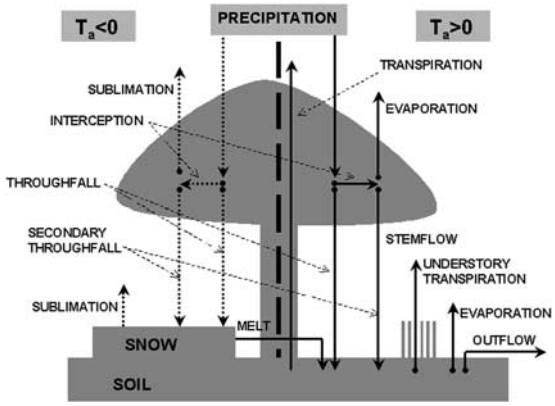

Figure 1. Water fluxes that are modeled in BEPS. When air temperature (T_a) is above zero, the water fluxes are illustrated in solid lines on the right side. Otherwise, the water fluxes are illustrated in dashed lines on the left side. At the top, precipitation is differentiated between rain and snow by air temperature (T_a).

Table 4); γ is the psychrometric constant (=0.646 + 0.0006 × T_a where T_a is the air temperature); and λ_v is the latent heat of vaporization of water dependent on air temperature (= (2.501 − 0.0024 × T_a) × 10^6 in J kg^{-1}); r_s is the surface resistance to water vapor, taken as the stomatal resistance of plants for individual leaves, which can be described in a combined function of radiation, air temperature, air humidity, and soil moisture, such as that of *Liu et al.* [1999].

[9] A convenient way of scaling up T_{plant} from leaf to canopy using the Penman-Monteith equation is to replace r_s with a canopy resistance. After the replacement, equation (2) becomes a 'big leaf model'. Big-leaf models were found adequate for ET estimation, but biased for estimating canopy photosynthesis [*Chen et al.*, 1999; *Lai et al.*, 2000]. Big-leaf ET models need to be adjusted for variable canopy architecture between various vegetation types. In particular, boreal forests are typically highly clumped. To be consistent with the carbon component of BEPS, we developed a canopy ET model with stratification of sunlit and shaded leaves. The consistency is particularly important when transpiration is used as the additional constraint on the estimation of gross primary productivity of a stand. Therefore T_{plant} can be simply described as follows:

$$T_{plant} = T_{sun}\mathrm{LAI}_{\mathrm{sun}} + T_{shade}\mathrm{LAI}_{\mathrm{shade}} \tag{3}$$

where T represents transpiration from leaves, and LAI is the leaf area index (see section 2.2.2 for LAI definition). The subscripts "sun" and "shade" denote the sunlit and shaded leaves, which are calculated from [*Chen et al.*, 1999]:

$$\mathrm{LAI}_{\mathrm{sun}} = 2\cos\theta[1 - \exp(-0.5\Omega\mathrm{LAI}/\cos\theta)] \tag{4a}$$

$$\mathrm{LAI}_{\mathrm{shade}} = \mathrm{LAI} - \mathrm{LAI}_{\mathrm{sun}} \tag{4b}$$

where θ is the daily mean solar zenith angle; Ω the clumping index, taken to be 0.5, 0.65, 0.8 and 0.9 for conifer, mixed forest, deciduous and other types (grass, cropland, tundra, etc.), respectively [*Liu et al.*, 1997].

[10] The Penman-Monteith equation is also used for estimating transpiration from the understory of forest. The understory transpiration is usually neglected in previous models but its contribution to total ET is found to be considerable in forest areas [*Black and Kelliher*, 1989]. Determination of a key parameter, understory LAI, is discussed in Section 2.2.2.

[11] Evaporation and sublimation from plants are dependent on the intercepted precipitation (rain or snow) (P_{int}) by plants and available energy to convert the solid or liquid water to vapor. The former is simply assumed to be proportional to leaf area index, constrained by precipitation:

$$P_{int} = \min(\mathrm{LAI}\ b_{int}, \mathrm{Precipitation}) \tag{5}$$

where b_{int} is a precipitation interception coefficient of 0.3 mm LAI^{-1} day^{-1} [*Running and Coughlan*, 1988]; the function *min* takes the minimum of the two outputs. When air temperature is above zero, evaporation occurs; otherwise, sublimation takes place. Therefore the following equations are use to estimate evaporation and sublimation, respectively:

$$E_{plant} = \min(S_{int}b_{abs\_water}/\lambda_v, P_{int}) \tag{6}$$

$$S_{plant} = \min(S_{int}b_{abs\_snow\_new}/\lambda_s, P_{int}) \tag{7}$$

where b_{abs_water} is the absorptivity to solar radiation for water, taking 0.50 [*Burman and Pochop*, 1994]; $b_{abs\_snow\_new}$ is the absorptivity to solar radiation for new snow, taking 0.1 [*Oke*, 1990]; λ_v is the latent heat of vaporization (= 2.5×10^6 J kg^{-1} at 0°C). λ_s is the latent heat of sublimation (= 2.8×10^6 J kg^{-1} at 0°C). S_{int} is the intercepted daily solar radiation in J m^{-2} day^{-1}, which is calculated with the consideration of the canopy architecture in terms of LAI and clumping index (Ω). The effect of solar zenith angle on S_{int} is integrated daily and a solution is found [*Liu et al.*, 1997]:

$$\begin{aligned} S_{int} &= S\left[(1-\rho_1) - (1-\rho_2)\left(\int_{\theta_{noon}}^{2/\pi} p(\theta)\cos\theta d\theta\right)\right. \\ &\quad \left.\Big/\left(\int_{\vartheta_{noon}}^{2/\pi} \cos\theta d\theta\right)\right] \\ &= S\left[(1-\rho_1) - (1-\rho_2)P(\theta_{noon})\right. \\ &\quad \left.\cdot\frac{\cos\theta_{noon} - \left(\frac{\pi}{2} - \theta_{noon}\right)\sin\theta_{noon}}{\left(\frac{\pi}{2} - \theta_{\mathrm{noon}}\right)(1-\sin\theta_{\mathrm{noon}})}\right] \end{aligned} \tag{8a}$$

$$P(\theta_{noon}) = e^{(-0.4\Omega\mathrm{LAI}/\theta noon)} \tag{8b}$$

where S is the daily total incoming solar radiation from the atmosphere in J m^{-2} day^{-1}. θ_{noon} is the solar zenith angle at noon and is a function of latitude and day of year [*Oke*, 1990]. $P(\theta_{noon})$ is the gap fraction at noon. ρ_1 and ρ_2 are reflectivities above and below the canopy and are assigned the values of 0.05 and 0.06, respectively [*Liu et al.*, 1997].

[12] Evaporation from soil (E_{soil}) is estimated with the Penman-Monteith equation for snow-free areas, whereas evaporation in snow covered areas is set to zero. The surface resistance in equation (2) is replaced with soil resistance to water vapor [*Monteith*, 1981; *Shuttleworth and Wallace*, 1985].

[13] If the snowpack exists on the ground, sublimation from snow is equal to the available energy to sublimate the existing snow:

$$S_{ground} = \min[\text{snow}, (S - S_{int})c_{snow}/\lambda_s] \quad (9)$$

where *snow* is snow water equivalent (mm); c_{snow} is a coefficient for the fraction of solar radiation transferred to latent heat by sublimation. It is around 0.12 for snow and ice [*Saunders et al.*, 1997].

[14] BEPS assumes the soil root zone to be a bucket of certain size. For each day, all water inputs to and outputs from the soil in a pixel are summed. If the total exceeds the water holding capacity in the root zone, water will flow out of the bucket. The total amount of excess water is treated as outflow.

2.2. Spatially Explicit Input Data

[15] As aforementioned, BEPS requires input data of land cover, leaf area index, available soil water holding capacity, and daily meteorological data. These data in spatially explicit form were prepared in a domain covering Canada with 5700 pixel by 4800 lines at 1 km resolution. The domain is in a Lambert conformal conic (LCC) projection (49° and 77°N standard parallels, 95°W meridian). All input data were processed into this resolution and projection before or during model execution. The year 1996 was selected to present a snapshot of annual ET pattern over the Canadian landmass.

2.2.1. Land Cover

[16] The information on land cover type is required to define the parameters describing individual biome types and to control model routines according to biome types. It is also useful in developing biome-dependent algorithms for the derivation of LAI maps described in section 2.2.2.

[17] The land cover map of Canada was generated to provide an up-to-date, spatially and temporally consistent national coverage. The data source is the Advanced Very High Resolution Radiometer (AVHRR) onboard NOAA 14 satellite. The data processing was carried out in the following steps: (1) conversion of raw AVHRR data into 10-day cloud-free composite products of top-of-atmosphere radiance; (2) transformation of the products in step 1 into refined composite products using a model dubbed ABC3 (atmospheric, bidirectional, and contamination corrections of CCRS, i.e., Canada Centre for Remote Sensing) [*Cihlar et al.*, 1997]; and (3) extraction of land cover information from step 2 composite data, using the Enhancement-Classification Method (ECM) [*Beaubien et al.*, 1999; *Cihlar et al.*, 1999]. The ABC3 performs the necessary steps of atmospheric correction, angular normalization (greatly reduces the noise due to large ranges of solar zenith angle and satellite view angle), and subpixel cloud/fog contamination detection and correction. ECM involves the steps of (1) reflectance histogram stretches (enhancement), (2) spectral clustering, (3) cluster merging, and (4) cluster labeling. Such an unsupervised classification method requires man-machine interactions in steps 3 and 4 and also allows for the use of ground evidence and operators' experience for accuracy improvement. The quality of the data set was assessed by a comparison with enhanced Landsat TM images at 30 km resolution and reviewed by scientists across the country. After comparing the map with Landsat TM images, *Klita et al.* [1998] found the preclass accuracy to vary between 21.8% and 97.9% in a forest region of central Canada, and *Pietroniro and Soulis* [1999] examined this map and other six land cover maps for the Mackenzie basin in Canada and ranked this map as having the highest overall accuracy. Some minor cover type have low accuracies at 1 km resolution in comparison with 30 m resolution because of the omission error, i.e., small areas disappear when mixed with dominant cover types in large pixels.

[18] The cover type of every land pixel is identified as one of ten classes based on the original 31 classes of *Cihlar et al.* [1999]. The ten classes include coniferous forest, mixed forest (mixture of coniferous and deciduous forest), deciduous forest, shrub land, burned area, barren land, cropland, grassland, urban area, and permanent snow/ice area. The variation of land cover with latitude is shown in Figure 2 for forest and other dominant types (Figure 2a) and for minor types (Figure 2b). Forested areas, especially coniferous forest, spread from the southern border of Canada to 66°N, with the highest density in 50°–54°N (Figure 2a). Dominant cover types in the north were barren land and snow- or ice- covered areas, diminishing gradually southward (Figure 2a). The latitudinal distribution patterns of crop land and shrub land show a maximum around 50°–54°N. Urban areas were scattered mostly in the south below 54°N, while burnt areas appeared more in the north.

2.2.2. Leaf Area Index (LAI)

[19] Leaf area index is defined as half the total leaf area (including all leaf sides) per unit ground surface [*Chen and Black*, 1992]. The algorithms for different land cover types have been developed in earlier studies [*Chen and Cihlar*, 1996; *Liu et al.*, 1999]. These algorithms were further improved and validated [*Chen et al.*, 2002]. A group of scientists made ground measurements in deciduous, mixed, coniferous forests, and cropland at several locations cross Canada. Eight Landsat TM scenes at 30 m resolution were used to locate ground sites and to facilitate spatial scaling to 1 km AVHRR pixel of AVHRR images. The accuracy of LAI values of individual pixels was found to be about 75%. The algorithms for LAI derivation and validation are given by *Chen et al.* [2002]. Atmospheric correction was found to be the most critical to the accuracy, and the relatively high accuracy was achieved through the use of pixel-matching daily water vapor, ozone and atmospheric pressure data. Compared with some earlier studies, our approach avoided a prescribed maximum LAI for different biome types [e.g., *Sellers et al.*, 1996] and converted the reflectance signals received from satellite to LAI directly, rather than using the vegetation indices, that combine the signals in various forms [e.g., *Choudhury and DiGirolamo*, 1998].

[20] The LAI images were generated using the ten-day composite AVHRR images, the products in step 2 described in section 2.2.1, over a period from 11 April to 31 October that covers most of the growing season in Canada [*Liu et al.*, 2002]. In the nongrowing season when air temperature is around or below 0°C., the value of LAI is either zero for

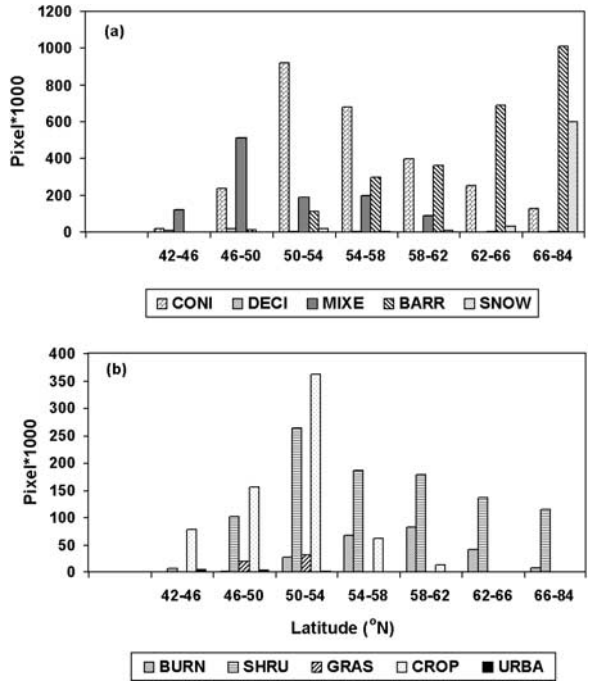

Figure 2. Land cover of Canada by latitude, (a) areas up to 1200 thousand pixels (1 pixel $\approx$ 1 km^2) for forest, barren land, and snow or ice area and (b) areas up to 400 thousand pixels for the rest of land cover types. CONI, coniferous forest; MIXE, mixed forest; DECI, deciduous forest; SHRU, shrub land; BURN, burnt area; BARR, barren land; CROP, cropland; GRAS, grassland; URBA, urban area; SNOW, snow/ice land.

crop and deciduous forest or nearly invariant for coniferous forest, mixed forest, grassland and shrubland. Therefore it is assumed that LAI before 11 April and after 31 October was the same as that on 11 April and 31 October, respectively.

[21] Figure 3 shows the seasonal variation of LAI averaged over different land cover types (Figure 3a) and the associated standard deviation (Figure 3b). In general, LAI values in Canada are lower than those in temperate or tropical regions due to its harsher climate. The annual mean LAI of three forests were comparable, while deciduous forest held the largest amplitude of variation as expected. The magnitude and seasonal variation of other land cover types were smaller than those of forests. Large standard deviations of LAI in Figure 3b arise from the large spatial extent of Canada where the vegetation density gradually decreases from high LAI values of southern forests to zero at the tree line in the north.

[22] BEPS treats a forest cover as two layers, overstory and understory. The LAI discussed above only includes overstory LAI for forests because the LAI algorithms were developed for overstory only. From measurements in the Boreal Ecosystem-Atmosphere Study (BOREAS) study [*Sellers et al.*, 1995], understory LAI of coniferous forest was found to be an exponential function of overstory LAI (Figure 4). Understory LAI for deciduous forest was variable in the range from 0.5 to 3.0 from field observations [e.g., *Black et al.*, 1996], and is set as a constant of 1.5 because no significant correlation between the overstory and undersotry LAI was found. Understory LAI for mixed forest, a mixture of coniferous and deciduous forests, was an average of understory LAI of coniferous forest (using the formula in Figure 4) and that of deciduous forest (a constant). It is understood that understory LAI is highly variable, and the methods used here only provide crude estimates of this layer of vegetation, which has a notable contribution to the total transpiration [*Black and Kelliher*, 1989], so we choose to include it rather than ignoring this difficult component. To set understory LAI of deciduous forest as a constant may affect 3–4% overall ET of this land cover (see Table 4 in section 3.4).

2.2.3. Soil Data

[23] The available soil water holding capacity (AWC) is the portion of water in the soil that can be readily extracted by plant roots. It is the water held in the root zone between field capacity and wilting point, a pressure of up to approximately 15 bars [*Shields et al.*, 1991]. The data of AWC were available in the Soil Landscapes of Canada (SLC) database, version 1.0 [*Shields et al.*, 1991]. AWC data are stored in polygon format on different files for each province. The original AWC data from each file were combined and processed to match land cover and LAI data at the same resolution and projection in a geographic information system (ARC/INFO). There are some gaps in AWC data set, mostly north of 70°N. *Kucharik et al.* [2000], in a global ecosystem model, related soil texture to the corresponding field capacity and the wilting point. This relationship is used to fill in AWC data gaps with texture data in SLC version 2.0.

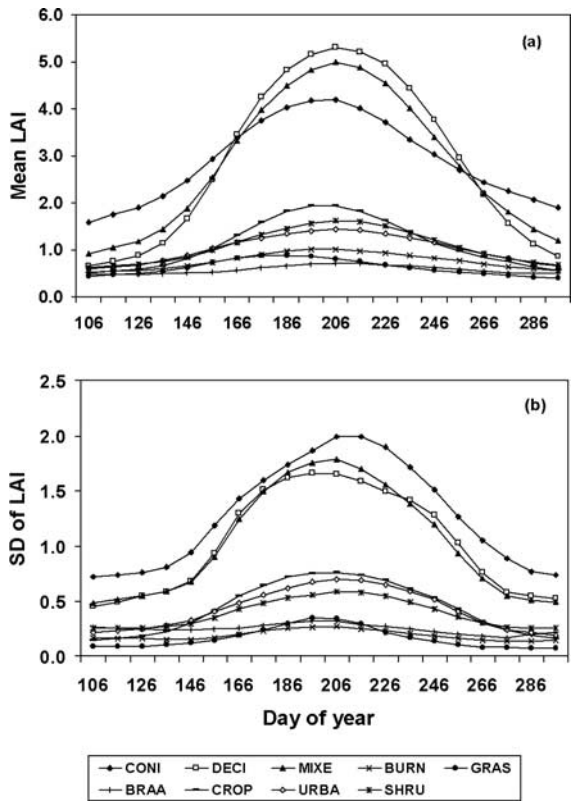

Figure 3. Temporal variation of LAI in different land cover types in the growing season of 1996 (a) mean and (b) stand deviation (SD). The legends are the same as those in Figure 2.

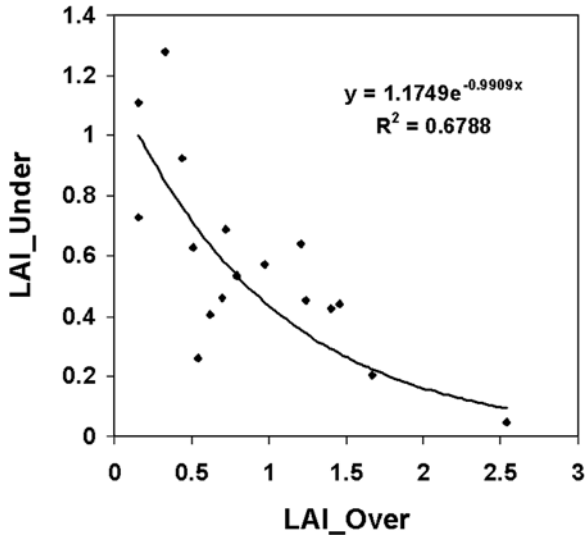

Figure 4. The relationship of understory LAI to overstory LAI for coniferous forest stands using an empirical equation based on field measurements in Saskatchewan and Manitoba.

[24] The national mean of AWC in forested areas is 0.11 m, while the mean values of AWC of cropland and grassland are 0.17 m and 0.16 m, respectively. Mean AWC of all land pixels is 0.13 m. The coefficient of variation, i.e., percentage of stand deviation over mean, is within 7% for each mean [*Liu et al.*, 2002].

2.2.4. Meteorological Data

[25] The daily meteorological data include global radiation, minimum and maximum temperatures, mean humidity and total precipitation, plus snowpack data at the beginning of a year. These data in gridded format were acquired from the National Center for Atmospheric Research (NCAR). The data were generated from the medium range forecast (MRF) Global Flux Archive [*Kalnay et al.*, 1990; *Kanamitsu*, 1989; *Kanamitsu et al.*, 1991] in the National Center for Environmental Prediction (NCEP), previously as National Meteorological Center (NMC). The original data have a grid size of ~0.9°, varying slightly with longitude and latitude, in a Gaussian grid system. All the meteorological variables were bilinearly interpolated into 1 km resolution and LCC projection as other input data for each pixel during the model execution.

[26] In order to evaluate the NCAR dataset, a comparison was made between the NCAR data and the observed meteorological data at 96 stations across Canada in 1996. The daily total radiation in NCAR data set was found 20–40% higher than the station measurement at the same location [*Liu et al.*, 1997, 2002]. This overestimation was corrected with a reduction coefficient for each month, determined with data from all stations. The mean reduction coefficient (standard deviation) from January to December 1996 was 0.68 (0.16), 0.66 (0.07), 0.74 (0.08), 0.71 (0.09), 0.74 (0.06), 0.77 (0.07), 0.78 (0.07), 0.81 (0.05), 0.68 (0.08), 0.62 (0.15), 0.59 (0.07), 0.50 (0.10). The yearly mean reduction coefficient was 0.69 with a stand deviation of 0.03. With over 30,000 pairs of data points, daily maximum temperature and minimum temperature in the NCAR dataset agree well with those of station data, with a correlation coefficient (R) of 0.93 for each, whereas the correlation coefficient for daily precipitation is only 0.62, indicating a large scatter. Annual statistics of temperature and precipitation were compared between the two data sets (Figure 5). For the mean maximum temperature averaged for a year at each station, 46% of stations had a difference smaller than 1°C between the two datasets, 64% of stations less than 3°C. The comparison is similar for the daily minimum temperature. The absolute difference between the two datasets averaged over all the stations was 1.9°C and 1.8°C for maximum and minimum temperatures, respectively. Annual total precipitation of NCAR data correlated with the station data better than daily total precipitation, with a correlation coefficient (R) of 0.75, although large discrepancies still remained, especially for stations where precipitation was about or over 1500 mm yr^{-1}. Mean annual precipitation averaged over all stations was 836 mm, in comparison with 863 mm of NCAR data. The absolute difference between the two datasets averaged for all the stations was 242 mm yr^{-1}. On the basis of the measure-

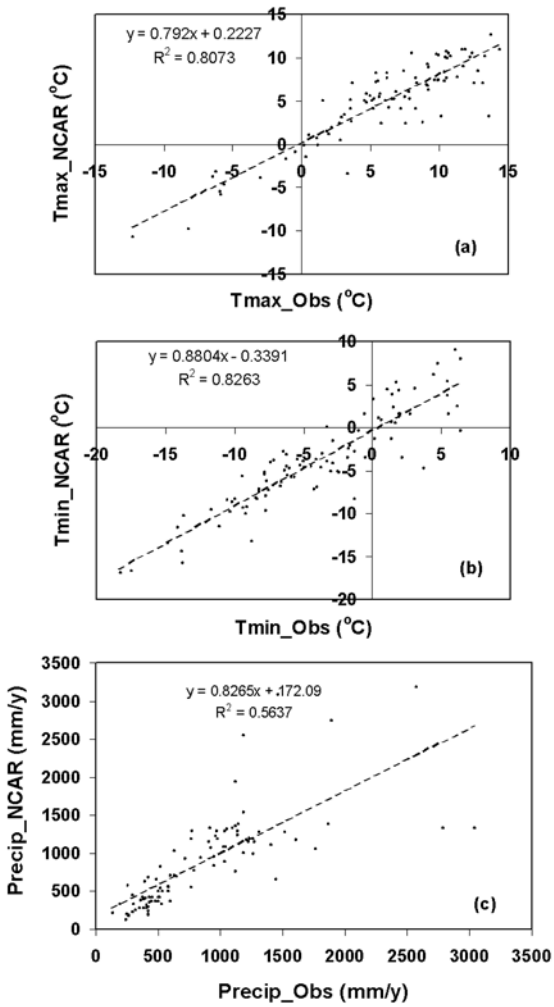

Figure 5. The comparison of (a and b) averaged daily maximum and minimum temperatures and (c) yearly total precipitation between these measured at the weather stations and those extracted from the NCAR data set at the same locations in 1996.

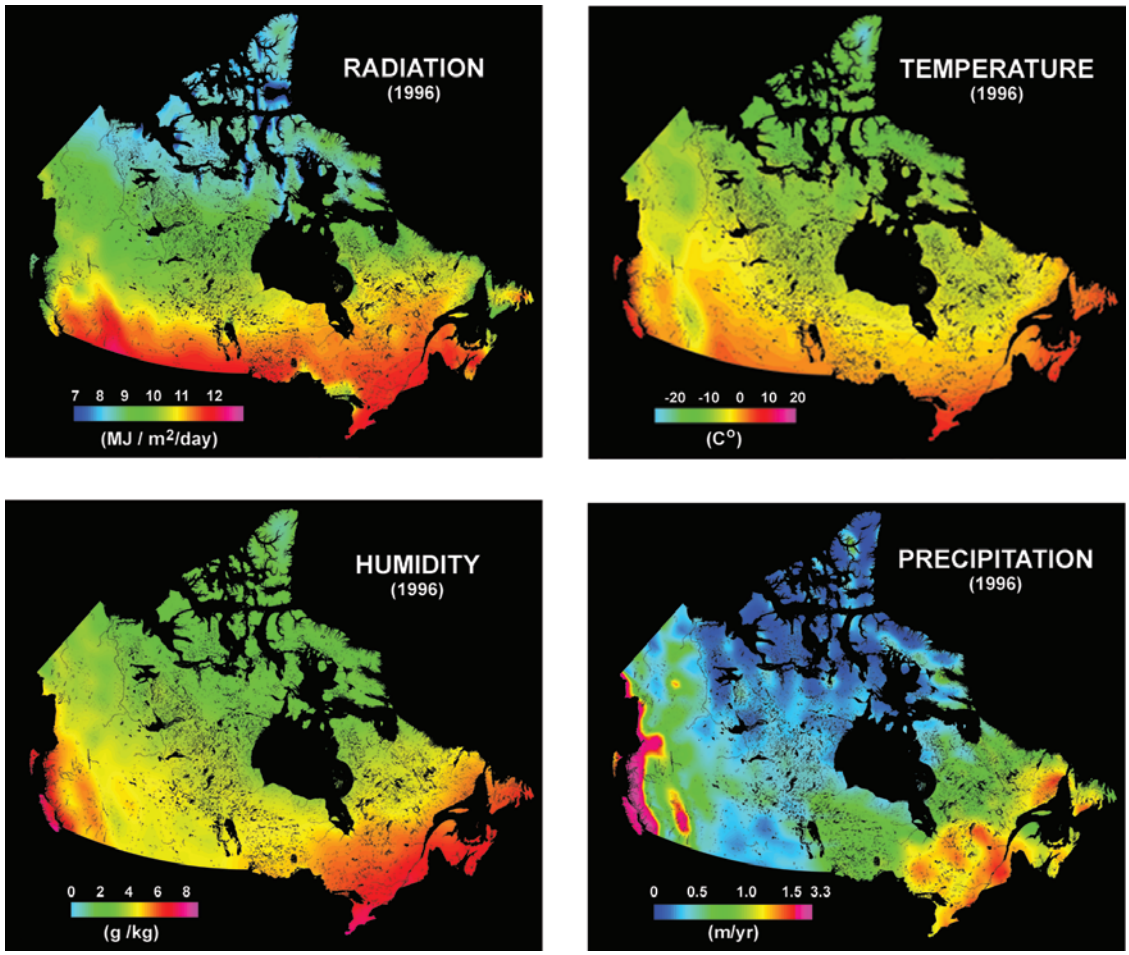

Figure 6. Distribution of meteorological variables in 1996: (top left) daily mean radiation in MJ m^{-2} day^{-1}, (top right) daily mean air temperature in °C, (bottom left) daily mean specific humidity in g kg^{-1}, and (bottom right) yearly total precipitation in mm yr^{-1}. National means of radiation, temperature, specific humidity and precipitation for 1996 were 9.9 MJ m^{-2} day^{-1}, −5.1°C, 4.2 g kg^{-1}, and 599 mm yr^{-1}, respectively.

ment of precipitation over North America, *Groisman and Easterling* [1994] found mean precipitation were 800–1000 mm yr^{-1} over 45–55°N and 400–600 mm yr^{-1} over 55–70°N from 1950 to 1990. The precipitation in NCAR data was 863 mm yr^{-1} averaged over 45–55°N and 436 mm yr^{-1}over 55–70°N, comparable to what Groisman and Easterling reported.

[27] Figure 6 shows Canada-wide distributions of global radiation, temperature, specific humidity, and precipitation in 1996, interpolated from NCAR data into 1 km resolution. The spatial patterns of these images are similar to the contour graphs for the long-term averages described by *Hare and Thomas* [1979] and *Hare* [1997]. Latitudinal gradients of radiation, temperature, and humidity were evident over Canada's landmass. Precipitation along two coasts was high, decreasing gradually toward inland, so was humidity below 60°N. This illustrates ocean's influence, while the cooler temperature over the Rocky Mountains reveals the topographical effect. National means of radiation, temperature, humidity and precipitation for 1996 were 9.9 MJ m^{-2} day^{-1}, −5.1°C, 4.2 g kg^{-1}, and 599 mm yr^{-1}, respectively. Note the annual precipitation averaged over Canada landmass from NCAR data was substantially lower than that measured at the weather stations because the most stations were located at southern latitudes, i.e. 51% in 42°–50°N, 39% in 51°–60°N, and only 10% over 60°N. In comparison with long-term meteorological records, the national average air temperature for 1996 was normal with a departure of 0.0°C from the mean of the 1948–2000 period, while the precipitation was 8.8% higher than the 53-year mean [*Environment Canada*, 2002].

2.3. Site Data for Model Comparison

[28] During the Boreal Ecosystem-Atmosphere Study (BOREAS) experiment [*Sellers et al.*, 1995], the water vapor flux was measured using the eddy covariance method at various sites [*Black et al.*, 1996; *Goulden et al.*, 1997; *Jarvis et al.*, 1997]. This provides a valuable database for model validation. The raw flux data were extracted and summed to daily totals at the flux tower sites for a whole year in 1994 when the extensive field campaigns were taken place and made such data available. Meteorological data including radiation, air temperature, humidity and precipitation were also extracted from the same data set and processed into daily values for the same time, where

available. Missing data were supplemented with the meteorological data from NCAR data set in 1994.

3. Results and Discussion

3.1. Model Comparison With Site Measurements

[29] Based on a previous intercomparison and evaluation of nine ecosystem process models at a black spruce site [*Amthor et al.*, 2001], a further comparison between modeled and measured ET values was made in this study at two additional sites, an old aspen site and another old black spruce site in the region. Figure 7 shows the overall results at the three sites. It appears that the model captures about 60% of the variations in the measurements with a root mean square error of 0.4, 0.7, 0.9 mm/day for the three sites, respectively. The model generally followed the measured seasonal patterns of ET with many pronounced drying events at the sites. The departure from the measurement may be due to the simplification of natural processes in the model, especially extreme subdaily transpiration and rainfall interception events.

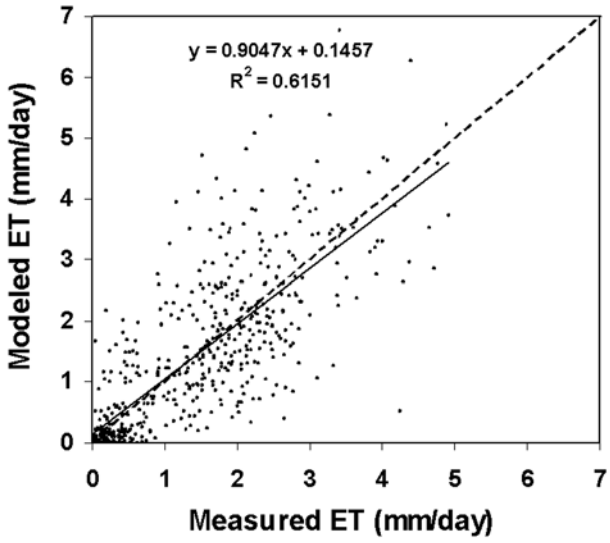

Figure 7. Comparison of the measured and the modeled daily ET over three forest stands.

3.2. Spatial Distribution of ET

[30] BEPS-simulated ET over Canada in 1996 is shown in Figure 8. The highest ET occurred in deciduous and mixed forests south of 50°N. The lowest ET values appeared over the vast ice/snow areas in the north and high-altitude Rocky Mountains along the west coast. It appears that the model was able to capture the combined effects of meteorology, soil, and vegetation on spatial patterns of ET distribution. Examples include (1) the latitudinal decrease of ET resulted mainly from available energy; (2) ET limitation by precipitation in the provinces of Alberta and Saskatchewan; and (3) higher ET values in forested areas than those of urban and suburban areas, even under similar meteorological conditions such as on the Vancouver Island. (Note the digital form of the ET map shows much greater details.)

[31] *Hare* [1980] derived a contour map of ET in Canada below 60°N from the difference between the precipitation and runoff in long-term records. The magnitude and overall pattern of ET distribution in this study are comparable to those of *Hare* [1980], in term of latitudinal and longitudinal distributions. However, a much more heterogeneous ET distribution is presented in this study on pixel basis instead of broad contours. Inspecting all input data, it is observed that the heterogeneity mainly resulted from variable vegetation type and density detected by satellite. Compared with Hare's method, BEPS can produce an ET map for specific periods (days, months, and years) so that both short- and long- term trends can be analyzed.

[32] Figure 9 shows the mean ET variations with longitude and latitude. The variation of ET with latitude was larger than that with longitude because of stronger latitudinal variations in meteorological conditions, vegetation type and density. The ET averaged over Canadian land surface was 228 mm yr^{-1} in 1996, partitioned into transpiration of 102 mm yr^{-1} and evaporation of 126 mm yr^{-1}. The spatial pattern of the ET/precipitation ratio (Figure 10) is similar to that identified by *Hare* [1980], who used the ratio of runoff to precipitation for the region below 60°N. Examining the ratio of ET to precipitation along longitude, high values are found in central Canada, decreasing toward both coasts (Figure 11). The amplitude of the variation is even larger for the mean below 60°N than that over all latitudes. The national mean ET/precipitation was 38% for 1996. Taking into account 8,933,436 land pixels in the domain, the total ET for 1996 is calculated as 2037 km^3, while the precipitation is 5351 km^3 yr^{-1} over the landmass.

[33] The subcomponents of transpiration, evaporation and the total ET are listed in Table 1. Transpiration from plants (overstory for forest), and evaporation from soil were most dominant components in ET, followed by evaporation from plants, and sublimation from the ground surface. Sublimation at air temperature below zero accounted for 23% of total evaporation. The understroy contributed 8% of the total transpiration nationally, while in forested areas, its contribution accounted for 15% of the total transpiration.

3.3. ET by Land Cover

[34] The spatial distribution of ET simulated by BEPS varies largely with land cover type. Table 2 shows that high ET values were associated with vegetated areas, ranging from 200 to 500 mm yr^{-1}. ET values over burnt, barren, urban, and snow areas were low, ranging from 60 to 200 mm yr^{-1}. Measured ET values in term of yearly totals are very limited in Canada. *Black et al.* [1996] and *Blanken et al.* [2001] reported that about 410 mm yr^{-1} of water was evaporated from an aspen stand at the BOREAS region in 1994. ET from some coniferous forest and fen sites at the BOREAS region during a growing season was measured to be 100–300 mm yr^{-1} [*Baldocchi et al.*, 1997; *Jarvis et al.*, 1997; *McCaughey et al.*, 1997a], revealing low ET values in boreal forest with possible reasons of shallow root zone and strong stomatal control on transpiration [*McCaughey et al.*, 1997b]. Summertime ET from 15 June to 25 August in a wetland site (58°40′N, 94°40′W) ranged from 100 to 300 mm yr^{-1} over a 10 year period, based on measurement and Bowen ratio-energy balance analysis [*Eaton and Rouse*, 2001]. *McCaughey* [1968] reported a potential ET of 241 mm from a crop land from 5 July to 5 September. In the energy and water study in the Mackenzie basin, where the dominant land cover was forest, estimated ET ranges

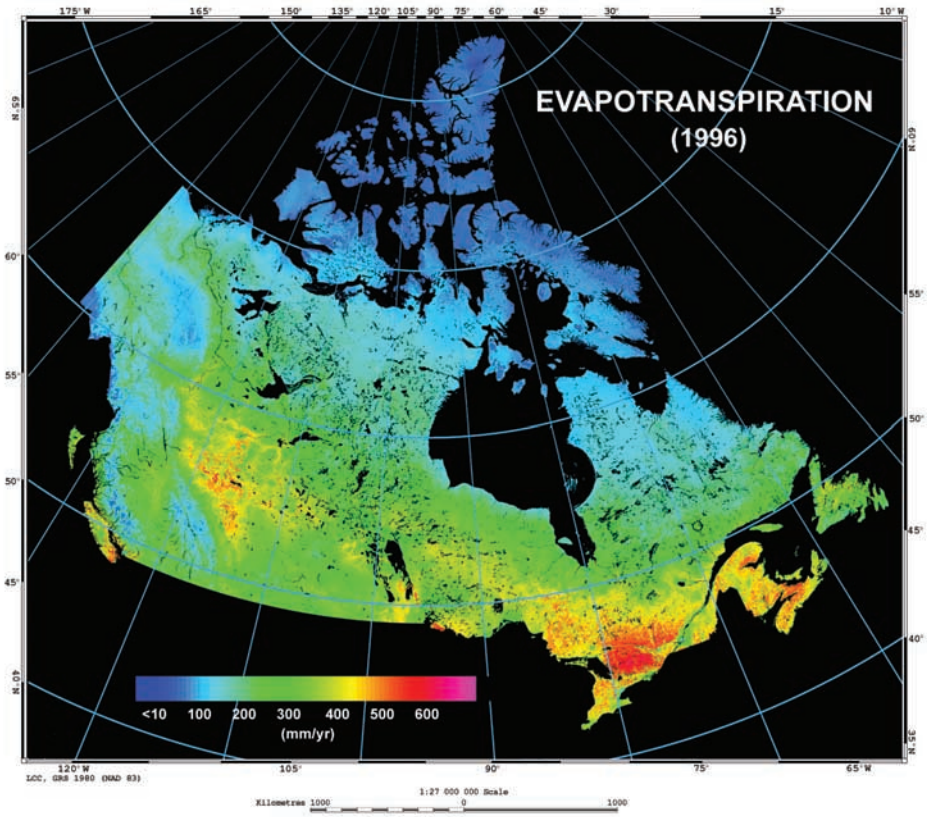

Figure 8. BEPS-simulated ET distribution over Canadian landmass in 1996.

between 87 to 277 mm yr^{-1} from different methods for various periods [*Stewart et al.*, 2002].

[35] Of the total ET, about 60% occurred in coniferous and mixed forests because of their large spatial extent and high ET flux density (Table 2). Cropland, shrub land, and barren land each contributed around 10–20% to the country-wide ET. The water loss from each of the rest of land cover types was less than 2% of the total national ET.

[36] The ratio of ET to precipitation depended on the distributions of both precipitation and land cover type (Table 3). For the whole landmass, the national mean ratio was high over cropland and grassland, intermediate for forests, and low for the rest of land cover types. As for the ratio of transpiration to ET, large differences between cover types also existed. Transpiration from vegetated surfaces attributed large fractions to ET. For nonvegetated or less vegetated land, transpiration became less dominant part of ET. The national mean transpiration/ET ratio was 45%, in comparison with 51% for forested areas.

3.4. Characteristics of BEPS, Uncertainties, and Future Work

[37] In BEPS, plant characteristics, including the vegetation type, density and canopy architecture, are taken into account in simulating various processes controlling ET. BEPS considers the Canadian environment with large forested and permafrost areas and long winter seasons. For example, the importance of the spatial variation in snow interception and sublimation with conifer stand density [*Pomeroy and Goodison*, 1997] has been modeled using LAI imagery, and the contribution of understory to ET [*Black and Kelliher*, 1989] is considered explicitly. The spatial LAI, land cover, and soil data are generated specifically for Canada, not extracted from other global data at coarser or the same resolutions. Compared with the ET maps from previous studies at continental or global scale with spatial resolutions of 2.8°–5° or in contour form [e.g., *Hare*, 1980; *Choudhury et al.*, 1998], the distribution of ET presented here shows spatial details that have not been seen prior to this study. Using remote sensing imagery with a moderate spatial resolution is essential for depicting such spatial details. To resolve problems due to limitations of data availability and computing resources, emphases of our study was placed on enhancing the spatial resolution rather than the temporal resolution. As the land surface is highly heterogeneous, such high-spatial resolution simulations would be a direction for improving regional ET estimation.

[38] Despite the ability of the model in capturing major characteristics of ET distribution, there are uncertainties arising from different sources. One of them is the uncertainty in spatial input data. Error estimates and their impacts on ET are given in Table 4. The impact of an error (positive or negative) in each variable was estimated through executing the model with the same percentage of change in the variable for all pixels throughout the year while keeping all other variables unchanged from their original input values. The combined error from all inputs can be additive or compensatory. The same relative change in a given variable can induce greater or smaller changes in ET in different regions than the national mean shown in Table 4. The

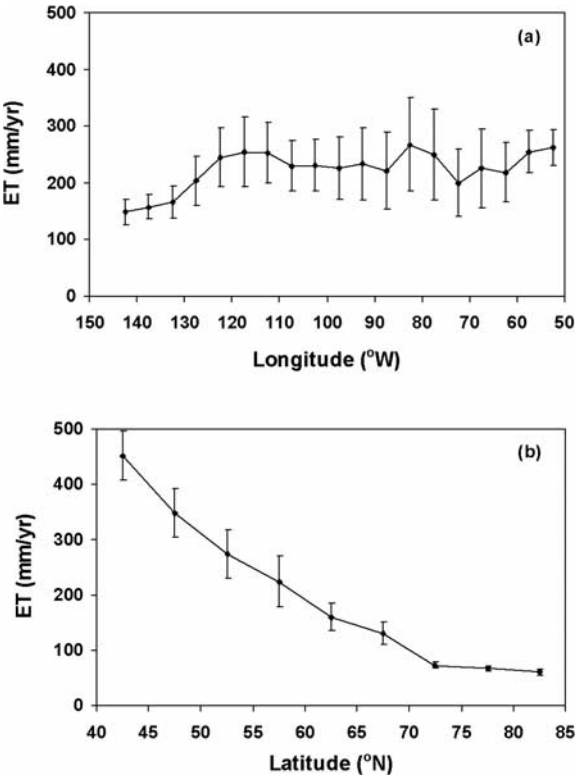

Figure 9. The variation of ET with (a) longitude and (b) latitude (mean and standard deviation in 5° intervals).

accuracies in LAI and land cover maps have considerable impacts on ET estimation. Errors in meteorological variables, which may be the upper bounds for a given region, can cause errors in ET of similar magnitudes. In dry regions of prairie provinces, the impact of ±25% errors in precipitation on ET is ±12–13%, about 3 times larger than the national average. In these regions, the uncertainty in precipitation data remains a major problem, a widely recognized common problem for regional and global evapotranspiration studies [*World Meteorological Organization* (*WMO*), 1993]. Biases can be caused by the treatments to simplify natural processes in the model, some of which are similar to those in other models at a comparable spatial scale [*Sellers et al.*, 1986; *Choudhury and DiGirolamo*, 1998]. Nevertheless, it appears from an intercomparison of nine models that model complexity and time step size might play small roles in monthly and annual estimation [*Amthor et al.*, 2001]. Another source of error may come from neglecting the effects of subpixel and subdaily variations. This can be addressed in the future when more spatial data, e.g., continuous fractional land cover maps [*DeFries et al.*, 1999], and enhanced computer capacity becomes available. It would also be highly desirable to have coincident ET data for further model and map validation for various cover types. The ''flat-Earth'' approach [*Sellers et al.*, 1986; *Dickinson et al.*, 1991] adopted in this study may affect the estimated ET spatial distribution in mountainous regions. This effect will also need to be evaluated through considering the lateral water redistribution among neighboring pixels [*Band et al.*, 1991; *Kouwen et al.*, 1993; *Wigmosta et al.*, 1994].

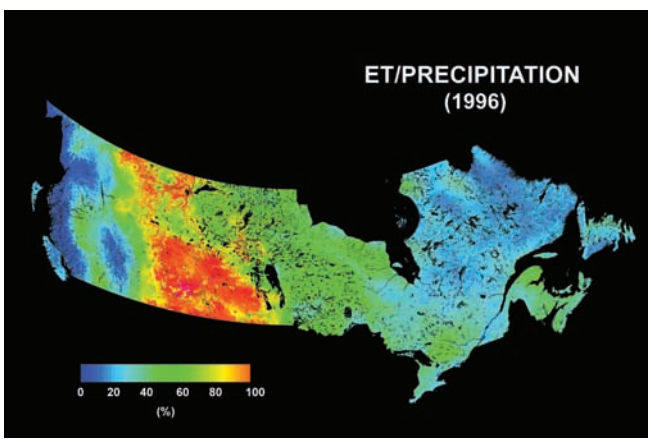

Figure 10. The spatial distribution of ratio of ET to precipitation in 1996 below 60°N. The ET/precipitation is capped at 100%, which includes cases of the ratio being over 100%.

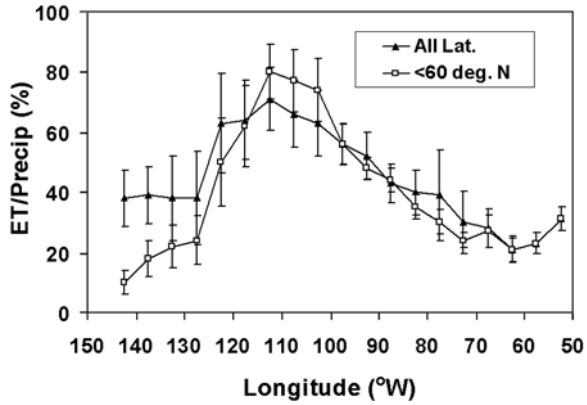

Figure 11. The longitudinal variation of the ratio of ET to precipitation in 1996 (mean and standard deviation in 5° intervals for all latitudes and the latitudes south of 60°N).

4. Summary

[39] Through the use of remote sensing and ancillary data, we were able to show the detailed spatial distribution patterns of evapotranspiration, an important hydrological component required for climate and water resources studies.

Table 1. BEPS-Simulated ET by Subcomponent

Component[a]	Mean, mm yr^{-1}	Sub./ET, %	Sub./Transp., %	Sub./Evap., %
T_{plant}	94	41	92	
T_{under}	8	4	8	
E_{plant}	38	17		30
E_{soil}	59	26		47
S_{plant}	8	4		6
S_{ground}	21	9		17
ET	228	100		
Transpiration	102	45	100	
Evaporation	126	55		100

[a]As defined in equation (1), T_{plant} is transpiration from plants or overstory plants (trees) for forested areas; T_{under} is transpiration of the understory in forests, equal to zero for nonforest cover types; E_{plant} and S_{plant} are evaporation and sublimation from plants, respectively; E_{soil} is evaporation from soil; and S_{ground} is sublimation from the snow on the ground. Total evaporation here include both evaporation and sublimation.

Table 2. BEPS-Simulated ET by Land Cover[a]

Land Cover	Number of Pixels	Class Mean ET, mm yr^{-1}	Class Total ET, km^3 yr^{-1}	Class/Total, %
Coniferous forest	2642329	276 (71)	730	36
Mixed forest	1121650	405 (78)	455	22
Deciduous forest	40240	492 (86)	20	1
Shrub land	986365	195 (51)	192	9
Burnt area	225228	184 (30)	42	2
Barren land	2496086	126 (32)	314	15
Cropland	670235	341 (63)	228	11
Grassland	51615	275 (42)	14	1
Urban area	9211	195 (32)	2	0
Snow/Ice land	690477	51 (7)	35	2
Forest	3804219	317 (96)	1204	59
Land	8933436	228 (120)	2037	100

[a]"Forest" refers to all forest pixels, including coniferous forest, mixed forest, and deciduous forest. "Land" refers to all Canadian land pixels, excluding water body. 1 pixel $\approx$ 1 km^2. The brackets are the standard deviation.

Table 4. Error Analysis on Input Data and Some Parameters in the Model[a]

Variable	Test Range		Effect on National ET	
	Low	High	Low	High
Radiation	−10%	+10%	−2%	+3%
Temperature	−1°C	+1°C	−8%	+11%
Specific humidity	−10%	+10%	+10%	−8%
Precipitation	−25%	+25%	−4%	+5%
LAI	−25%	+25%	−8%	+10%
AWC	−25%	+25%	−7%	+8%
r_a	−50%	+50%	−3%	+4%
$LAI_{deci,\ under}$	−1.0	+1.0	−3%	+4%
Land cover	25% CONI to DECI		+7%	
Land cover	25% DECI to CONI		−0.1%	
Land cover	25% CONI to BRAA		−5%	
Land cover	25% BRAA to CONI		3%	
Land cover	25% CONI to CROP		1%	
Land cover	25% CROP to CONI		−0.4%	

[a]The results of $LAI_{deci,under}$ only show the effect of the change on the ET of deciduous forest only. The effect on the national ET is much less than 1%. The testing on land cover is made only for dominant, unmixed vegetation types, or land cover types. CONI, coniferous forest; DECI, deciduous forest; BARR, barren land; CROP, cropland.

The major components of the process model used for ET mapping were validated using water flux measurements at three forested sites. The ET distribution results from both the surface and atmospheric conditions. The former are mostly detected by satellite and the latter are quantified by gridded datasets, after removing random and bias errors from these data sets to the extent possible in comparison with meteorological station data. Therefore both the spatial distribution patterns and the mean values of ET found in this study represent independent and new information.

[40] Remote sensing data at a moderate spatial resolution, when used as driving variables for the process model, enable us to simulate actual ET at that resolution over large areas, a significant step forward from estimating the potential ET from climatic data. Without vegetation type and density data derived from remote sensing, the simulation of the actual ET in such detail would not be possible. The spatial explicit information on ET is useful in estimating surface water balance and soil moisture for large areas and predicting hydrographs for large river basins, particularly before and during flood events. In addition, it should facilitate runoff estimation for ungauged or small watersheds in support of hydroelectric power generation.

[41] As remote sensing, meteorology, and other relevant disciplines advance rapidly, substantial improvements in spatial ET estimation can still be made in the near future. Better characterization of subpixel land cover heteorogeneity and seasonal dynamics, better gridded precipitation data, shorter modeling time steps, higher spatial resolution of remote sensing images, and further refinements of the process models are among the main directions to improve spatial mapping of ET near real-time.

Appendix A: Methods for Net Radiation Estimation

[42] BEPS calculates the net radiation of the sunlit and shaded leaves for the overstory separately:

$$R^*_{sun} = S^*_{sun} + L^*_{sun}, \tag{A1a}$$

$$R^*_{shade} = S^*_{shade} + L^*_{shade} \tag{A1b}$$

where the capital symbols of S and L represent shortwave and longwave irradiances, respectively; superscript asterisk

Table 3. ET/Precipitation and Transpiration/ET by Land Cover[a]

Land Cover	Precipitation, mm yr^{-1}	Transpiration, mm yr^{-1}	Evaporation, mm yr^{-1}	ET/Precipitation, %	Transpiration/ET, %
Coniferous forest	686 (358)	123 (55)	153 (34)	40	45
Mixed forest	1001 (462)	244 (64)	162 (35)	40	60
Deciduous forest	1175 (448)	327 (69)	165 (33)	42	67
Shrub land	731 (479)	68 (38)	127 (19)	27	35
Burnt area	479 (255)	57 (20)	127 (16)	38	31
Barren land	392 (305)	23 (18)	102 (18)	32	18
Cropland	509 (355)	231 (50)	110 (27)	67	68
Grassland	314 (137)	191 (38)	83 (14)	88	70
Urban area	1182 (594)	62 (22)	133 (13)	16	32
Snow/ice land	284 (396)	0 (0)	51 (7)	18	0
Forest	784 (420)	161 (81)	156 (35)	40	51
Land	599 (434)	102 (94)	126 (40)	38	45

[a]"Forest" refers to all forest pixels, including coniferous forest, mixed forest, and deciduous forest. "Land" refers to all Canadian land pixels, excluding water body. The brackets are the standard deviation.

denotes the net radiation component and the subscripts sun and shade denote sunlit leaves and shaded leaves, respectively. Downward flux is defined as positive conventionally. Methods for calculating the shortwave radiation components are based on *Chen et al.* [1999] for calculating visible radiation, but is modified for total solar radiation. The partition of incoming solar radiation into direct and diffuse components is done using the following equations:

$$\frac{S_{dif}}{S_g} = \begin{cases} 0.943 + 0.734r - 4.9r^2 + 1.796r^3 + 2.058r^4 & r < 0.8 \\ 0.13 & r \geq 0.8 \end{cases} \quad \text{(A2a)}$$

$$S_{dir} = S_g - S_{dif} \quad \text{(A2b)}$$

where S_g is the incoming global radiation in W m^{-2}, the parameter r is defined as:

$$r = \frac{S_g}{S_0 \cos\theta} \quad \text{(A3)}$$

where S_0 and θ are the solar constant (= 1367 W m^{-2}) and solar zenith angle, respectively.

[43] The sunlit leaf net radiance (S^*_{sun}) is calculated as [*Norman*, 1982]:

$$S^*_{sun} = (1 - \alpha_L)(S_{dir} \cos\alpha / \cos\theta) + S^*_{shade} \quad \text{(A4)}$$

where α_L is leaf scattering coefficient (taken as a constant of 0.25); α is mean leaf-sun angle. $\alpha = 60°$ for a canopy with spherical leaf angle distribution, which is found to be also a good approximation for boreal canopies in θ range from 30° to 60° [*Chen*, 1996]. The method for estimating the mean shaded leaf irradiance (S^*_{shade}) is as follows:

$$S^*_{shade} = \left(S_{dif} - S_{dif,under}\right)/\mathrm{LAI} + \mathrm{C} \quad \text{(A5)}$$

where $S_{dif,under}$ is diffuse radiation under the overstory; C arises from multiple scattering of direct radiation. An equation for calculating C is derived based on *Norman* [1982] with a modification by *Chen et al.* [1999]:

$$C = \alpha_L \Omega S_{dir}(1.1 - 0.1\mathrm{LAI}) \exp(-\cos\theta) \quad \text{(A6)}$$

where Ω is the foliage clumping index. Equation (A5) states that diffuse irradiance on shaded leaves originates from two sources: sky irradiance and multiple scattering of the incident radiation within the canopy. The first term in equation (A5) makes the average of the total intercepted diffuse radiation from the sky for the total LAI involved (sunlit leaves also contribute to the interception). The diffuse radiation reaching to the soil surface is calculated using the simple equation with the consideration of the clumping effect:

$$S_{dif,under} = S_{dif} \exp\left(-0.5\Omega \mathrm{LAI_o} / \cos\bar{\theta}_o\right) \quad \text{(A7)}$$

where the subscripts o denotes overstory, in comparison with u for understory in equation (A13) and others, and $\mathrm{LAI_o}$ = LAI. $\bar{\theta}_o$ is a representative zenith angle for diffuse radiation transmission and slightly dependent on leaf area index:

$$\cos\bar{\theta}_o = 0.537 + 0.025\mathrm{LAI_o}. \quad \text{(A8)}$$

This is a simple but an effective way to calculate the transmitted diffuse radiation. It avoids the integration of the sky irradiance for the hemisphere by using a representative transmission zenith angle $\bar{\theta}_o$, which is obtained through a numerical experiment with the complete integration. Under the assumption of isotropic sky radiance distribution, it is near a constant of 57.5° but also a weak function of overstory LAI (LAI_o). This angle is larger than the mean of 45° because the hemisphere is more heavily weighted against the lower sphere in the integration. The dependence on overstory LAI is found because it modifies slightly the weight distribution.

[44] For the understory, no separation between the sunlit and shaded leaves are made and the net radiation is calculated from

$$R^*_u = S^*_u + L^*_u. \quad \text{(A9)}$$

Similarly, for the ground surface underneath the vegetation layers, net radiation is:

$$R^*_g = S^*_g + L^*_g. \quad \text{(A10)}$$

The net shortwave radiation of the understory is calculated as

$$S^*_u = (1 - \alpha_L)\left(S_{dir} e^{-0.5\mathrm{LAI_0}\Omega/\cos\theta} + S_{dif,under}\right), \quad \text{(A11)}$$

and the net shortwave radiation of the ground is calculated as

$$S^*_g = \left(1 - \alpha_g\right)\left(S_{dir} e^{-0.5(\mathrm{LAI}_o + \mathrm{LAI}_u)\Omega/\cos\theta} + S_{dif,under} e^{-0.5\mathrm{LAI}_u\Omega/\cos\bar{\theta}_u}\right) \quad \text{(A12)}$$

where α_g is the albedo of the ground surface taken as a constant of 0.2, and the representative angle for diffuse radiation transmission through the understory is estimated in a similar way as equation (A8):

$$\cos\bar{\theta}_u = 0.537 + 0.025\mathrm{LAI}_u \quad \text{(A13)}$$

[45] A system of equations for calculating net longwave radiation of the vegetation layers and the ground surface is developed in this study. For the overstory, net longwave exchanges of sunlit and shaded leaves are treated the same, i.e.,

$$L^*_{sun} = L^*_{shade} = \frac{L^*_o}{\mathrm{LAI}_o} \quad \text{(A14)}$$

A more elaborate formulation can be made to consider the temperature difference between sunlit and shaded leaves. However, our sensitivity tests suggest that detailed calculations of leaf energy budget and temperature can make only less than 1% difference in terms of the final ET. The net

longwave irradiances for the overstory (L_o^*), understory (L_u^*), and the soil surface (L_g^*) are calculated using the following equations:

$$L_o^* = \left\{\varepsilon_o\left[\varepsilon_a\sigma T_a^4 + \varepsilon_u\sigma T_u^4\left(1 - e^{-0.5\mathrm{LAI}_u\Omega/\cos\overline{\theta_u}}\right) + \varepsilon_g\sigma T_g^4 e^{-0.5\mathrm{LAI}_u\Omega/\cos\overline{\theta_u}}\right] - 2\varepsilon_o\sigma T_o^4\right\}\left(1 - e^{-0.5\mathrm{LAI}_o\Omega/\cos\overline{\theta_o}}\right) \quad \text{(A15)}$$

$$L_u^* = \left\{\varepsilon_u\left[\varepsilon_a\sigma T_a^4 e^{-0.5\mathrm{LAI}_o\Omega/\cos\overline{\theta_o}} + \varepsilon_o\sigma T_o^4\left(1 - e^{-0.5\mathrm{LAI}_O\Omega/\cos\overline{\theta_O}}\right) + \varepsilon_g\sigma T_g^4\right] - 2\varepsilon_u\sigma T_u^4\right\}\left(1 - e^{-0.5LAI_u\Omega/\cos\overline{\theta_u}}\right) \quad \text{(A16)}$$

$$L_g^* = \varepsilon_g\left\{\left[\varepsilon_a\sigma T_a^4 e^{-0.5\mathrm{LAI}_o\Omega/\cos\overline{\theta_o}} + \varepsilon_o\sigma T_u^4\left(1 - e^{-0.5\mathrm{LAI}_o\Omega/\cos\overline{\theta_o}}\right)\right]e^{-0.5\mathrm{LAI}_u/\cos\overline{\theta_u}} + \varepsilon_u\sigma T_u^4\left(1 - e^{-0.5\mathrm{LAI}_u\Omega/\cos\overline{\theta_u}}\right)\right\} - \varepsilon_g\sigma T_g^4 \quad \text{(A17)}$$

where ε_a, ε_o, ε_u, and ε_g are emissivities of the atmosphere, overstory, understory and ground surface, respectively. Predescribed values of 0.98, 0.98 and 0.95 are assigned to ε_o, ε_u, and ε_g, respectively, according to [*Chen and Zhang*, 1989; *Chen et al.*, 1989], and ε_a is computed as $\varepsilon_a = 1.24\left(\frac{e_a}{T_a}\right)^{\frac{1}{7}}$ [*Brutsaert*, 1982], where e_a and T_a are water vapor pressure in mb and temperature of the atmosphere in K. For daily step calculations, we assume that $T_g = T_a = T_u = T_o$. The representative angles for longwave transmission through the overstory and understory are treated the same as those for diffuse radiation transmission described in equations (A8) and (A13).

[46] **Acknowledgments.** The authors wish to thank David Fraser, Rasim Latifovic, Wenjun Chen, Goran Pavlic, Bill Park, and Mike Sarich for their help in the model development and data processing over the past several years. Data from the BOREAS database, Agriculture and Agri-Food Canada, and the U.S. National Center for Atmospheric Research are acknowledged. This study is part of the Northern Biosphere Observation and Modeling Experiment (NBIOME). The financial support of the Canadian Space Agency is gratefully acknowledged.

References

Amthor, J. S., et al., Boreal forest CO_2 and water vapor exchanges predicted by nine ecosystem process models: Model results and relationships to measured fluxes, *J. Geophys. Res.*, *106*, 33,623–33,648, 2001.

Baldocchi, D. D., C. A. Vogel, and B. Hall, Seasonal variation of energy and water vapor exchange rates above and below a boreal jack pine forest canopy, *J. Geophys. Res.*, *102*, 28,939–28,952, 1997.

Band, L. E., D. L. Peterson, S. W. Running, J. C. Coughlan, R. Lammers, J. Dungan, and R. R. Nemani, Ecosystem processes at the watershed level: Basis for distributed simulation, *Ecol. Modell.*, *56*, 171–196, 1991.

Beaubien, J., J. Cihlar, G. Simard, and R. Latifovic, Land cover from multiple Thematic Mapper scenes using a new enhancement: Classification methodology, *J. Geophys. Res.*, *104*, 27,909–27,920, 1999.

Black, T. A., and F. M. Kelliher, Process controlling understorey evapotranspiration, *Philos. Trans. R. Soc. London, Ser. B*, *324*, 207–231, 1989.

Black, T. A., et al., Annual cycle of water vapour and carbon dioxide fluxes in and above a boreal aspen forest, *Global Change Biol.*, *2*, 101–111, 1996.

Blanken, P. D., T. A. Black, H. H. Neumann, G. den Hartog, P. C. Yang, Z. Nesic, and X. Lee, The seasonal water and energy exchange above and within a boreal aspen forest, *J. Hydrol.*, *245*, 118–136, 2001.

Braud, A. C. D., M. Vauclin, J. L. Thony, and P. Ruelle, A simple soil-plant-atmosphere transfer model (SiSPAT) development and field verification, *J. Hydrol.*, *166*, 213–250, 1995.

Brutsaert, W. H., *Evaporation Into the Atmosphere*, D. Reidel, Norwell, Mass., 1982.

Burman, R., and L. O. Pochop, *Evaporation, Evapotranspiration and Climate Data*, Elsevier Sci., New York, 1994.

Chan, D., J. Liu, K. Yuen, K. Higuchi, J. Chen, and J. Cihlar, The coupling of a three-dimensional regional atmospheric model to a biospheric CO_2 flux model, paper presented at International Science Conference: The Role of Boreal Forests and Forestry in the Global Carbon Budget, Nat. Resour. Can., Edmonton, Alberta, 8–12 May 2000.

Chan, D., K. Yuen, J. Liu, A. Shashkov, K. Higuch, and J. Chen, Simulation of the exchange processes between the biosphere and atmosphere at the regional scale using a coupled atmosphere-ecosystem model, paper presented at the 6th International Carbon Dioxide Conference, World Meteorol. Organ., Sendai, Japan, 1–5 Oct. 2001.

Chen, J. M., Canopy architecture and remote sensing of the fraction of photosynthetically active radiation in boreal conifer stands, *IEEE Trans. Geosci. Remote Sens.*, *34*, 1353–1368, 1996.

Chen, J. M., and T. A. Black, Defining leaf area index for non-flat leaves, *Plant Cell Envrion.*, *15*, 421–429, 1992.

Chen, J. M., and J. Cihlar, Retrieving leaf area index for boreal conifer forests using landsat TM images, *Remote Sens. Environ.*, *55*, 153–162, 1996.

Chen, J. M., and R. H. Zhang, Studies on the measurements of crop thermal emissivity and sky temperature, *Agric. For. Meteorol.*, *49*, 23–34, 1989.

Chen, J. M., B. J. Yang, and R. H. Zhang, Soil thermal emissivity as affected by its water content and surface treatment, *Soil Sci.*, *148*, 433–435, 1989.

Chen, J. M., J. Liu, J. Cihlar, and M. L. Goulden, Daily canopy photosynthesis model through temporal and spatial scaling for remote sensing applications, *Ecol. Modell.*, *124*, 99–119, 1999.

Chen, J. M., et al., Validation of Canada-wide leaf area index maps using ground measurements and high and moderate resolution satellite imagery, *Remote Sens. Environ.*, *80*, 165–184, 2002.

Choudhury, B. J., Estimating areal evaporation using multispectral satellite observations, in *Land Surface Processes in Hydrology, Trials and Tribulations of Modeling and Measuring*, edited by S. Sorooshian, H. V. Gupta, and J. C. Rodda, pp. 347–382, Springer-Verlag, New York, 1997.

Choudhury, B. J., and N. E. DiGirolamo, A biophysical process-based estimate of global land surface evaporation using satellite and ancillary data: I. Model description and comparison with observations, *J. Hydrol.*, *205*, 164–185, 1998.

Choudhury, B. J., N. E. DiGirolamo, J. Susskind, W. L. Darnell, S. K. Gupta, and G. Asrar, A biophysical process-based estimate of global land surface evaporation using satellite and ancillary data: II. Regional and global patterns of seasonal and annual variations, *J. Hydrol.*, *205*, 186–204, 1998.

Cihlar, J., J. M. Chen, and Z. Li, Seasonal AVHRR multichannel data sets and products for studies of surface-atmosphere interactions, *J. Geophys. Res.*, *102*, 29,625–29,640, 1997.

Cihlar, J., J. Beaubien, R. Latifovic, and G. Simard, Land cover of Canada 1995 version 1.1: Digital data set documentation, Nat. Resour. Can., Ottawa, Ontario, 1999. (Available at ftp://ftp2.ccrs.nrcan.gc.ca/ftp/ad/EMS/landcover95/).

DeFries, R. S., J. R. G. Townshend, and M. Hansen, Continuous fields of vegetation characteristics at the global scale, *J. Geophys. Res.*, *104*, 16,911–16,925, 1999.

Dickinson, R. E., A. Henderson-Sellers, C. Rosenzweig, and P. J. Sellers, Evapotranspiration models with canopy resistance for use in climate models, A review, *Agric. For. Meteorol.*, *54*, 373–388, 1991.

Eaton, A. K., and W. R. Rouse, Control of evapotranspiration at a subarctic sedge fen, *Hydrol. Proc.*, *15*, 3423–3431, 2001.

Environment Canada, Climate trends and variation bulletin for Canada, Ottawa, Ontario, 2002. (Available at http://www.msc-smc.ec.gc.ca/ccrm/bulletin/national_e.cfm).

Grace, J., *Plant-Atmosphere Relationships*, Chapman and Hall, New York, 1983.

Goulden, M. L., B. C. Daube, S.-M. Fan, D. J. Sutton, A. Bazzaz, J. W. Munger, and S. C. Wofsy, Physiological responses of a black spruce forest to weather, *J. Geophys. Res.*, *102*, 28,987–28,996, 1997.

Groisman, P. Y., and D. R. Easterling, Variability and trends of total precipitation and snowfall over the United States and Canada, *J. Clim.*, *7*, 184–205, 1994.

Hare, F. K., Long-term annual surface heat and water balances over Canada and the United States south of 60°N: Reconciliation of precipitation, runoff and temperature field, *Atmos. Ocean*, *18*, 127–153, 1980.

Hare, F. K., Canada's climate: An overall perspective, in *The Surface Climates of Canada*, edited by W. G. Bailey, T. R. Oke, and W. R. Rouse, pp. 3–20, McGill-Queen's Univ. Press, Montreal, Canada, 1997.

Hare, F. K., and M. K. Thomas, *Climate Canada*, 2nd ed., John Wiley, New York, 1979.

Henning, D., *Atlas of the Surface Heat Balance of the Continents*, Gebruder Borntraeger, Berlin, 1989.

Jarvis, P. G., J. M. Massheder, S. E. Hale, J. B. Moncrieff, M. Rayment, and S. L. Scott, Seasonal variation of carbon dioxide, water vapor, and energy exchanges of a boreal black spruce forest, *J. Geophys. Res.*, *102*, 28,953–28,966, 1997.

Jiang, L., and S. Islam, Estimation of surface evaporation map over southern Great Plains using remote sensing data, *Water Resour. Res.*, *37*, 329–340, 2001.

Kalnay, E., M. Kanamitsu, and W. E. Baker, Global numerical weather prediction at the National Meteorological Center, *Bull. Am. Meteorol. Soc.*, *71*, 1410–1428, 1990.

Kanamitsu, M., Description of the NMC global data assimilation and forecast system, *Weather Forecasting*, *4*, 335–342, 1989.

Kanamitsu, M., J. C. Alpert, K. A. Campana, P. M. Caplan, D. G. Deaven, M. Iredell, B. Katz, H.-L. Pan, J. Sela, and G. H. White, Recent changes implemented into the global forecast system at NMC, *Weather Forecasting*, *6*, 425–435, 1991.

Kite, G. W., and A. Pietroniro, Remote sensing application in hydrological modelling, *Hydrol. Sci.*, *41*, 563–591, 1996.

Klita, D. L., R. J. Hall, J. Cihlar, J. Beaubien, K. Dutchak, R. Nesby, J. Drieman, R. Usher, and T. Perrott, A comparison between two satellite-based land cover classification programs for a boreal forest region in northwest Alberta, Canada, paper presented at the 20th Canadian Symposium on Remote Sensing, Can. Remote Sens. Soc., Calgary, Alberta, May 1998.

Kouwen, N., E. D. Soulis, A. Pietroniro, J. Donald, and R. A. Harrington, Grouping response units for distributed hydrologic modelling, *J. Water Resour. Manage. Plann.*, *119*, 289–305, 1993.

Kucharik, C. J., J. A. Foley, C. Delire, V. A. Fisher, M. T. Coe, J. D. Lenters, C. Young-Molling, N. Ramankutty, J. M. Norman, and S. T. Gower, Testing the performance of a dynamic global ecosystem model: Water balance, carbon balance and vegetation structure, *Global Biogeochem. Cycles*, *14*, 795–825, 2000.

Kuittinen, R., Remote sensing for hydrology process and prospects, *Operational Hydrol. Rep. 36*, World Meteorol. Organ., Geneva, Switzerland, 1992.

Lai, C., G. Katul, R. Oren, D. Ellswoth, and K. Schafer, Modeling CO_2 and water vapor turbulent flux distributions within a forest canopy, *J. Geophys. Res.*, *105*, 26,333–26,351, 2000.

Liu, J., J. M. Chen, J. Cihlar, and W. M. Park, A process-based boreal ecosystem productivity simulator using remote sensing inputs, *Remote Sens. Environ.*, *62*, 158–175, 1997.

Liu, J., J. M. Chen, J. Cihlar, and W. Chen, Net primary productivity distribution in the BOREAS region from a process model using satellite and surface data, *J. Geophys. Res.*, *104*, 27,735–27,754, 1999.

Liu, J., J. M. Chen, and J. Cihlar, Estimating Canada-wide evapotranspiration based on remote sensing, paper presented at the 7th Annual Scientific Meeting of the Mackenzie GEWEX Study (MAGS), Nat. Sci. and Eng. Res. Counc. (NSERC) of Can., Hamilton, Ontario, 7 –9 Nov. 2001.

Liu, J., J. M. Chen, J. Cihlar, and W. Chen, Net primary productivity mapped for Canada at 1-km resolution, *Global Ecol.*, 11,115–129, 2002.

McCaughey, J. H., A test of the Penman combination model for potential evaporation, *Publ. Climatol. 1*, McMaster Univ., Hamilton, Ontario, Canada, 1968.

McCaughey, J. H., P. M. Lafleur, D. W. Joiner, P. A. Bartleet, A. M. Costello, D. E. Jelinski, and M. G. Ryan, Magnitudes and seasonal patterns of energy, water, and carbon exchanges at a boreal young jack pine forest in the BOREAS northern study area, *J. Geophys. Res.*, *102*, 28,997–29,007, 1997a.

McCaughey, J. H., B. D. Amiro, A. W. Robertson, and D. Spittlehouse, Forest environments, in *The Surface Climates of Canada*, edited by W. G. Bailey, T. R. Oke, and W. R. Rouse, pp. 247–276, McGill-Queen's Univ. Press, Montreal, Canada, 1997b.

Monteith, J. L., Evaporation and environment, *Symp. Soc. Exp. Biol.*, 205–234, 1965.

Monteith, J. L., Evaporation and surface temperature, *Q. J. R. Meteorol. Soc.*, *107*, 1–27, 1981.

Mintz, Y., and G. K. Walker, Global fields of soil moisture and land surface evapotranspiration derived from observed precipitation and surface air temperature, *J. Appl. Meteorol.*, *32*, 1305–1334, 1993.

Norman, J. M., Modeling the complete crop canopy, in *Modification of the Aerial Environment of Plants*, edited by B. J. Barfield and J. F. Gerber, pp. 249–277, Am. Soc. of Agric. Eng., St. Joseph, Mich., 1979.

Norman, J. M., Simulation of microclimates, in *Biometeorology in Integrated Pest Management*, edited by J. L. Hatfield and I. J. Thomason, pp. 65–99, Academic, San Diego, Calif., 1982.

Oke, T. R., *Boundary Layer Climates*, 2nd ed., Routledge, New York, 1990.

Pauwels, V. R. N., and E. F. Wood, A soil-vegetation-atmosphere transfer scheme for the modeling of water and energy balance processes in high latitudes: 1. Model improvements, *J. Geophys. Res.*, *104*, 27,711–27,822, 1999.

Pietroniro, A., and E. D. Soulis, Assessment of global land-cover data for atmospheric and hydrologic model applications in the Mackenzie basin, Canada, paper presented at the 5th Scientific Workshop for the Mackenzie GEWEX study, Nat. Sci. and Eng. Res. Counc. (NSERC) of Can., Edmonton, Alberta, 21 –23 Nov. 1999.

Pomeroy, J. W., and B. E. Goodison, Winter and snow, in *The Surface Climates of Canada*, edited by W. G. Bailey, T. R. Oke, and W. R. Rouse, McGill-Queen's Univ. Press, Montreal, Canada, 1997.

Potter, C. S., J. T. Randerson, C. B. Field, P. A. Matson, P. M. Vitousek, H. A. Mooney, and S. A. Klooster, Terrestrial ecosystem production: a process model based on global satellite and surface data, *Global Biogeochem. Cycles*, *7*, 811–841, 1993.

Potter, C., et al., Comparison of boreal ecosystem model sensitivity to variability in climate and forest site parameters, *J. Geophys. Res.*, *106*, 33,671–33,688, 2001.

Rango, A., (Ed.), *Remote Sensing and Large-Scale Global Processes*, *IAHSPubl.*, vol. 186, Int. Assoc. Hydrol. Sci., Wallingford, UK, 1989.

Rango, A., and A. I. Shalaby, Urgent operational applications of remote sensing in hydrology, *Operational Hydrol. Rep. 43*, World Meteorol. Organ., Geneva, Switzerland, 1999.

Running, S. W., and J. C. Coughlan, A general model of forest ecosystem processes for regional applications: I. Hydrological balance, canopy gas exchange and primary production processes, *Ecol. Modell.*, *42*, 125–154, 1988.

Running, S. W., R. R. Nemani, D. L. Peterson, L. E. Band, D. F. Potts, L. L. Pierce, and M. A. Spanner, Mapping regional forest evapotranspiration and photosynthesis by coupling satellite data with ecosystem simulation, *Ecology*, *70*, 1090–1101, 1989.

Saunders, I. R., D. S. Munro, and W. G. Bailey, Alpine environments, in *The Surface Climates of Canada*, edited by W. G. Bailey, T. R. Oke, and W. R. Rouse, pp. 222–246, McGill-Queen's Univ. Press, Montreal, Canada, 1997.

Seguin, B., Areal evaporation from satellite thermal infrared data, in *Land Surface Processes in Hydrology, Trials and Tribulations of Modeling and Measuring*, edited by S. Sorooshian, H. V. Gupta, and J. C. Rodda, pp. 318–309, Springer-Verlag, New York, 1997.

Sellers, P. J., Y. Mintz, Y. C. Sue, and A. Dalcher, A simple biosphere model (SiB) for use within general circulation models, *J. Atmos. Sci.*, *43*, 505–531, 1986.

Sellers, P., et al., The boreal ecosystem-atmosphere study (BOREAS): An overview and early results from the 1994 field year, *Bull. Am. Meteorol. Soc.*, *76*, 1549–1577, 1995.

Sellers, P. J., S. O. Los, C. J. Tucker, C. O. Justice, D. A. Dazlich, G. J. Collatz, and D. A. Randall, A revised land surface parameterization (SiB2) for atmospheric GCMs. part II: The generation of global fields of terrestrial biophysical parameters from satellite data, *J. Clim.*, *9*, 706–737, 1996.

Shuttleworth, W. J., and J. S. Wallace, Evaporation from sparse crops—A energy combination theory, *Q. J. R. Meteorol. Soc.*, *111*, 839–855, 1985.

Shields, J. A., C. Tarnocai, K. W. G. Valentine, and K. B. MacDonald, *Soil Landscapes of Canada, Procedures Manual and User's Hand Book. Publ. 1868/E*, Agric. Canada, Ottawa, Ontario, 1991.

Sorooshian, S., H. V. Gupta, and J. C. Rodda (Eds.), *Land Surface Processes in Hydrology, Trials and Tribulations of Modeling and Measuring*, Springer-Verlag, New York, 1997.

Stewart, J. B., E. T. Engman, R. A. Feddes, and Y. Kerr (Eds.), *Scaling up in Hydrology Using Remote Sensing*, John Wiley, New York, 1996.

Stewart, R. E., et al., Hydrometeorological features of the Mackenzie basin climate system during 1994/95 water year: A period of record low discharge, *Atmos. Ocean*, *40*, 257–278, 2002.

Strasser, U., and W. Mauser, Modelling the spatial and temporal variations of the water for the Weser catchment 1965–1994, *J. Hydrol.*, *254*, 199–214, 2001.

Wigmosta, M. S., L. W. Vail, and D. P. Lettenmaier, A distributed hydrology-vegetation model for complex terrain, *Water Resour. Res.*, *30*, 1665–1679, 1994.

Willmott, C. J., C. M. Rowe, and Y. Mintz, Climatology of the terrestrial seasonal water cycle, *J. Climatol.*, *5*, 589–606, 1985.

Wood, E. F., and V. Lakshmi, Scaling water and energy fluxes in climate systems: Three land-atmospheric modeling experiments, *J. Clim.*, *6*, 839–857, 1993.

World Meteorological Organization (WMO), Global observations, analyses and simulation of precipitation, *WMO/TD 544*, Geneva, Switzerland, 1993.

Zelic, A., J. M. Chen, J. Liu, and F. Csillag, Algorithms for spatial scaling of net primary productivity using subpixel information, paper presented at International Geoscience and Remote Sensing Symposium (IGARSS), IEEE Geosci. and Remote Sens. Soc., Toronto, Canada, 24–28 June 2002.

J. M. Chen, Department of Geography, University of Toronto, 100 St. George Street, Toronto, Ontario, Canada M5S 3G3. (chenj@geog.utoronto.ca)

J. Cihlar, Canada Centre for Remote Sensing, 588 Booth Street, Ottawa, Ontario, Canada K1A 0Y7. (josef.cihlar@ccrs.nrcan.gc.ca)

J. Liu, Atmospheric Science, Department of Physics, University of Toronto, 60 St. George Street, Toronto, Ontario, M5S 1A7. (jliu@atmosp.physics.utoronto.ca)